Computational Materials Science 53 (2012) 474–482

Contents lists available at SciVerse ScienceDirect

Computational Materials Science

journal homepage: www.elsevier.com/locate/commatsci

Grain growth prediction with inclination dependence of ⟨1 1 0⟩ tilt grain boundary using multi-phase-field model with penalty for multiple junctions

Tomoyuki Hirouchi [a], Tomohito Tsuru [b], Yoji Shibutani [c,*]

[a] JSPS Fellow, Graduate School of Mechanical Engineering, Osaka University, 2-1, Yamada-oka, Suita, 565-0871 Osaka, Japan
[b] Nuclear Science and Engineering Directorate, Japan Atomic Energy Agency, 2-4, Shirakata-Shirane, Tokai-mura, 319-1195 Ibaraki, Japan
[c] Department of Mechanical Engineering, Osaka University, 2-1, Yamada-oka, Suita, 565-0871 Osaka, Japan

ARTICLE INFO

Article history:
Received 11 August 2011
Received in revised form 24 August 2011
Accepted 25 August 2011
Available online 26 October 2011

Keywords:
Grain growth
Multi-phase-field model
Higher-order term
Grain boundary
Inclination dependence
Misorientation dependence

ABSTRACT

Multi-phase-field (MPF) model with a higher-order term representing energetic penalty for multiple junctions was proposed to predict the grain growth accompanying the inclination dependence of grain boundary (GB) energy and mobility. The inclination effect was introduced on the basis of GB energy obtained from molecular dynamics (MD) simulations. The preliminary grain growth simulation of an isolated grain surrounded by Σ3 GB certified that the analytical equilibrium shape was well reproduced. The augmented higher-order term added to conventional MPF model could improve convergence and stability of numerical calculations around triple junction (TJ) region even if there exists the large GB energy gap at the TJ. Moreover, the present MPF model can realize well the Young's relation with no GB inclination effect and further extend to the case with that effect. For the polycrystalline grain growth simulations with the GB energy distribution according to the misorientation angle of Al ⟨1 1 0⟩ tilt GB, Σ3 GB inclination lead the weak anisotropy characterized by Σ3{111} twin boundary. Besides, the inclination dependence can effectively drive the GBs with low GB energy like the low-angle GB during grain growth.

1. Introduction

Recently, innovative improvements of mechanical properties by strategically-designed inhomogeneous microstructures in metallic materials such as ultra-fine grains [1], nanotwins [2], bulk-nanometals [3] and so on have actively been discussed. Their internal structures include much higher density of grain boundary (GB) than conventional coarse-grain materials and maintain their quasi-stable states under mechanical balance among driving force for grain growth by elimination of GB regions and other effects like an internal stress field due to defects. Understanding in-depth grain growth mechanism via an effective modeling for not only the conventional macroscopic internal structures but also such novel microscopic ones should be therefore further developed. For the above-mentioned challenge, the more physically realistic modeling for grain growth predictions would be implemented into the phase field (PF) simulations which have been recognized as one of the prominent computational methodologies [4–7]. To that end, GB energy and mobility dependent on the misorientation and inclination angles, the latter of which is the deviation angle from the symmetric GB plane, are the things to be firstly considered.

Various computational models with the GB energy and mobility dependent on its misorientation and inclination have so far been proposed [8–15]. Their simulations with the energy anisotropy have shown that low-energy boundaries have high fraction after grain growth as supported by the experimental results [16–18]. These low-energy boundaries correspond to the low-angle and the coincidence site lattice boundaries (CSLs). The recent experiment [17] has shown that the inclination dependence of the GB energy affects the GB plane distribution to bulk structure and has confirmed an increase of low-energy GB plane. In this study, the multi-phase-field (MPF) model [19,20] with a higher-order term representing energetic penalty for multiple junctions, which can treat the stable triple junction (TJ) behavior accompanying the large difference between GB energies, is proposed incorporating the effect of inclination dependence of GB energy based on molecular dynamics (MD) simulations [21]. The preliminary grain growth simulations of isolated grain and tricrystal are carried out for certification of the present MPF model. On that numerical adequateness, polycrystalline grain growth simulations are performed using the proposed MPF model combined with the GB energy distribution based on the misorientation dependence of Al ⟨1 1 0⟩ tilt GB and discuss their contributions to grain growth process.

2. Numerical procedures

2.1. Multi-phase-field modeling

To consider a polycrystalline system including N grains, N non-conserved phase fields $\phi^1, \phi^2, \ldots, \phi^\alpha, \ldots, \phi^N$ are introduced to

* Corresponding author. Tel.: +81 6 6879 7310; fax: +81 6 6879 7247.
E-mail address: sibutani@mech.eng.osaka-u.ac.jp (Y. Shibutani).

0927-0256/$ - see front matter © 2011 Elsevier B.V. All rights reserved.
doi:10.1016/j.commatsci.2011.08.030

describe the system state of individual grain. They vary from 1 as inside the grain to 0 as the outside and between them as their overlapping states. The quantities of overlapping phase fields (grains), n, are recognized as grain ($n = 1$), GB ($n = 2$), TJ ($n = 3$), higher-order junction ($n \geqslant 4$) and so on, keeping the constraint of $\sum_{\alpha=1}^{n}\phi^{\alpha} = 1$. Based on the MPF concept [19], a free energy functional using these phase fields is given by,

$$\begin{aligned} &F(\phi^1,\phi^2,\ldots,\phi^N,\nabla\phi^1,\nabla\phi^2,\ldots,\nabla\phi^N)\\ &\quad=\int_V f(\phi^1,\phi^2,\cdots,\phi^3,\nabla\phi^1,\nabla\phi^2,\ldots,\nabla\phi^N)dV\\ &\quad=\int_V\left\{f_0+\sum_{\alpha=1}^{N}f_1^{\alpha}+\sum_{\alpha<\beta}^{N}f_2^{\alpha\beta}+\sum_{\alpha<\beta<\chi}^{N}f_3^{\alpha\beta\chi}+\cdots\right\}dV. \end{aligned} \tag{1}$$

This functional consists of the following components: f_0 contains energy independent of the phase state; f_1^{α} the energy difference between bulk phases; $f_2^{\alpha\beta}$ the energy of GB between phases α and β; $f_3^{\alpha\beta\chi}$ might correspond to the one of TJ and so on. Since the energy parts of TJ and higher-order junction are not explicitly expressed in the already proposed MPF model, the following free energy functional F is altered in the present study as,

$$F=\int_V\left[f_e+\sum_{\alpha<\beta}^{N}\left(-\frac{4\delta_{gb}\gamma^{\alpha\beta}}{\pi^2}\nabla\phi^{\alpha}\cdot\nabla\phi^{\beta}+\frac{4\gamma^{\alpha\beta}}{\delta_{gb}}\phi^{\alpha}\phi^{\beta}\right)+\sum_{\alpha<\beta<\chi}^{N}W^{\alpha\beta\chi}\phi^{\alpha}\phi^{\beta}\phi^{\chi}\right]dV, \tag{2}$$

where $\gamma^{\alpha\beta}$ is the energy of GB between grains α and β, $W^{\alpha\beta\chi}$ heights of the energy barrier with respect to TJ property, δ_{gb} GB thickness, and f_e free energy density in the grains. The second higher-order term of right-hand side would be related to TJ. Remind that the energy of TJ has not been fully understood [22] although it has been estimated experimentally [23]. Thus, we assume that parameter $W^{\alpha\beta\chi}$ is determined by the energies of GBs adjoining TJ (see Fig. 1(a)) with a weighting function F_w using the average GB energy $\bar{\gamma}=2\sum_{\alpha<\beta}^{n}\gamma^{\alpha\beta}/n(n-1)$ and the deviation $w_0=(\gamma^{\alpha\chi}-\bar{\gamma})/\bar{\gamma}$, as follows:

$$\begin{aligned} &W^{\alpha\beta\chi}=\frac{4\gamma^{\alpha\chi}}{\delta_{gb}}\times F_w(\text{at }\alpha\neq\beta\neq\chi),\\ &F_w=A\{3-\cos^4(w_0/2)-\cos^{16}(w_0/2)-\cos^{64}(w_0/2)\},\\ &A=\{3-\cos^4(w_m/2)-\cos^{16}(w_m/2)-\cos^{64}(w_m/2)\}^{-1}. \end{aligned} \tag{3}$$

where $|w_m| = 3$ is maximum of w_0. The weighing function is proportional to the deviation from the average GB energy. It converges to 1 as w_0 is close to w_m and must be set as 0 if there is not stable condition of $\gamma^{\beta\chi}/\sin\Theta^{\alpha}=\gamma^{\chi\alpha}/\sin\Theta^{\beta}=\gamma^{\alpha\beta}/\sin\Theta^{\chi}$, where Θ^{α} is the TJ angle, i.e. an inequality of $\gamma^{\alpha\beta}+\gamma^{\beta\chi}<\gamma^{\chi\alpha}$ at $n = 3$ is valid. This condition, of course, leads to eliminate a TJ with $\gamma^{\alpha\beta}+\gamma^{\beta\chi}<\gamma^{\chi\alpha}$ due to a wetting transition [24,25]. The above weighting function is continuous for $-w_m \leqslant w_0 \leqslant w_m$, as illustrated in Fig. 1(b). To create the inclination dependence of GB energy, let us consider $\gamma^{\alpha\beta}=\gamma^{\alpha\beta}(\Phi)$, where Φ is an inclination angle determined by local gradients of phase fields $\nabla\phi^{\alpha}$ and $\nabla\phi^{\beta}$ as shown in Fig. 2. Its definition will be explained in detail in Section 2.2. In the case of no inclination dependence of GB energy, the evolution equation of phase field ϕ^{α} can be derived as [20]

$$\begin{aligned} \frac{\partial\phi^{\alpha}}{\partial t}=-\frac{2}{n}\sum_{\beta=1}^{N}M(\phi)\Bigg[&-\frac{8}{\pi}\sqrt{\phi^{\alpha}\phi^{\beta}}\Delta E^{\alpha\beta}+\sum_{\chi=1}^{N}\Bigg\{\frac{4\delta_{gb}}{\pi^2}(\gamma^{\alpha\chi}-\gamma^{\beta\chi})\nabla^2\phi^{\chi}\\ &+\frac{4}{\delta_{gb}}(\gamma^{\alpha\chi}-\gamma^{\beta\chi})\phi^{\chi}+\sum_{\delta=1}^{N}(W^{\alpha\chi\delta}-W^{\beta\chi\delta})\phi^{\chi}\phi^{\delta}\Bigg\}\Bigg]. \end{aligned} \tag{4}$$

Taking the inclination dependence of GB energy into consideration, the evolution equation reduces to

$$\begin{aligned} &\frac{\partial\phi^{\alpha}}{\partial t}=-\frac{2}{n}\sum_{\beta=1}^{N}M(\phi)\left[-\frac{8}{\pi}\sqrt{\phi^{\alpha}\phi^{\beta}}\Delta E^{\alpha\beta}+\sum_{\chi=1}^{N}\left\{\frac{4\delta_{gb}}{\pi^2}\nabla\cdot((\gamma^{\alpha\chi}-\gamma^{\beta\chi})\nabla\phi^{\chi})+\frac{4}{\delta_{gb}}(\gamma^{\alpha\chi}-\gamma^{\beta\chi})\phi^{\chi}+\sum_{\delta=1}^{N}\left(W^{\alpha\chi\delta}-W^{\beta\chi\delta}\right)\phi^{\chi}\phi^{\delta}+B_1+B_2+B_3\right\}\right],\\ &B_1=\frac{4\delta_{gb}}{\pi^2}\frac{\partial}{\partial x}\left(\frac{\partial\gamma^{\alpha\chi}}{\partial\Phi}\frac{\partial\Phi}{\partial\phi^{\alpha}_{,x}}\nabla\phi^{\alpha}\nabla\phi^{\chi}-\frac{\partial\gamma^{\beta\chi}}{\partial\Phi}\frac{\partial\Phi}{\partial\phi^{\beta}_{,x}}\nabla\phi^{\beta}\nabla\phi^{\chi}\right)+\frac{4\delta_{gb}}{\pi^2}\frac{\partial}{\partial y}\left(\frac{\partial\gamma^{\alpha\chi}}{\partial\Phi}\frac{\partial\Phi}{\partial\phi^{\alpha}_{,y}}\nabla\phi^{\alpha}\nabla\phi^{\chi}-\frac{\partial\gamma^{\beta\chi}}{\partial\Phi}\frac{\partial\Phi}{\partial\phi^{\beta}_{,y}}\nabla\phi^{\beta}\nabla\phi^{\chi}\right),\\ &B_2=-\frac{4}{\delta_{gb}}\frac{\partial}{\partial x}\left(\frac{\partial\gamma^{\alpha\chi}}{\partial\Phi}\frac{\partial\Phi}{\partial\phi^{\alpha}_{,x}}\phi^{\alpha}\phi^{\chi}-\frac{\partial\gamma^{\beta\chi}}{\partial\Phi}\frac{\partial\Phi}{\partial\phi^{\beta}_{,x}}\phi^{\beta}\phi^{\chi}\right)-\frac{4}{\delta_{gb}}\frac{\partial}{\partial y}\left(\frac{\partial\gamma^{\alpha\chi}}{\partial\Phi}\frac{\partial\Phi}{\partial\phi^{\alpha}_{,y}}\phi^{\alpha}\phi^{\chi}-\frac{\partial\gamma^{\beta\chi}}{\partial\Phi}\frac{\partial\Phi}{\partial\phi^{\beta}_{,y}}\phi^{\beta}\phi^{\chi}\right),\\ &B_3=\sum_{\delta=1}^{N}\frac{\partial}{\partial x}\left(\frac{\partial W^{\alpha\chi\delta}}{\partial\Phi}\frac{\partial\Phi}{\partial\phi^{\alpha}_{,x}}\phi^{\alpha}\phi^{\chi}\phi^{\delta}-\frac{\partial W^{\beta\chi\delta}}{\partial\Phi}\frac{\partial\Phi}{\partial\phi^{\beta}_{,x}}\phi^{\beta}\phi^{\chi}\phi^{\delta}\right)+\sum_{\delta=1}^{N}\frac{\partial}{\partial y}\left(\frac{\partial W^{\alpha\chi\delta}}{\partial\Phi}\frac{\partial\Phi}{\partial\phi^{\alpha}_{,y}}\phi^{\alpha}\phi^{\chi}\phi^{\delta}-\frac{\partial W^{\beta\chi\delta}}{\partial\Phi}\frac{\partial\Phi}{\partial\phi^{\beta}_{,y}}\phi^{\beta}\phi^{\chi}\phi^{\delta}\right), \end{aligned} \tag{5}$$

where subscript $()_x$ and $()_y$ refer to deviation to x and y axes. $\partial f_e/\partial\phi^a-\partial f_e/\partial\phi^{\beta}=-\frac{8}{\pi}\sqrt{\phi^{\alpha}\phi^{\beta}}\Delta E^{\alpha\beta}$ is frequently used when the difference in free energy density of $\Delta E^{\alpha\beta}$ between grains α and β is taken into account. $\Delta E^{\alpha\beta}$ is defined as the difference of stored energy in each grain for recrystallization [6,7]. $8/\pi$ is obtained from $\int_0^1\sqrt{\phi^1\phi^2}d\phi=\int_0^1\sqrt{\phi(1-\phi)}d\phi=\frac{\pi}{8}$ so that this driving force in the GB region at $n = 2$ reduces to ΔE^{12}. The latter terms of B_1, B_2, B_3 are added to describe the effects of the inclination-dependent GB energy [26], and Eq. (5) reduces to Eq. (4) in the case without inclination dependence. In Eqs. (4) and (5), on an assumption that the mobility of multiple junction is dependent on that of GB connecting at the junction, the phase field mobility $M(\phi)$ is defined in this study as follows:

$$M(\phi)=\frac{\pi^2}{8\delta_{gb}}\frac{\sum_{\alpha<\beta}^{n}M^{\alpha\beta}\phi^{\alpha}\phi^{\beta}}{\sum_{\alpha<\beta}^{n}\phi^{\alpha}\phi^{\beta}}, \tag{6}$$

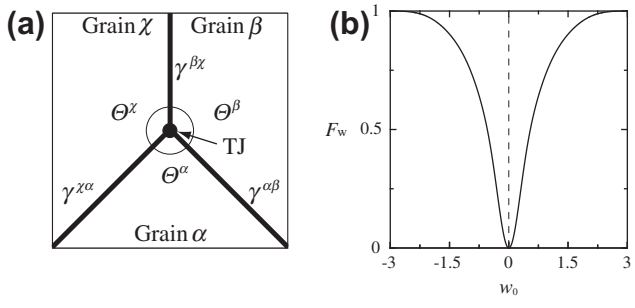

Fig. 1. (a) Relationship between GB energy $\gamma^{\alpha\beta}$ and TJ angle Θ^{α} at a TJ, and (b) the weighting function F_w as a function of the deviation from the average GB energy at a TJ.

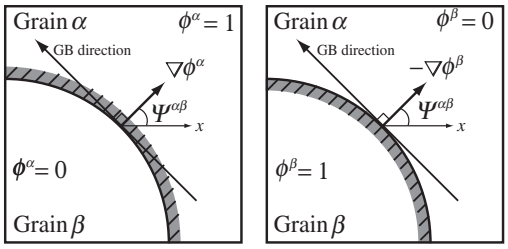

Fig. 2. Schematic illustration of GB inclination angle calculated by local gradients of the phase fields.

where $M^{\alpha\beta}$ is the mobility for α–β GB. Eq. (6) reduces to $\frac{\pi^2}{8\delta_{gb}}M^{\alpha\beta}$ for GB region ($n = 2$) and is averaged only for multiple junction's region ($n > 2$). Taking an average at the junction improves the convergence of numerical calculations around the junction. Meanwhile, it is a fact that there is numerically little difference between Eq. (6) and the conventional equation, which is recently supported by Ref. [27].

The numerical scheme employed here is based on an algorithm proposed by Kim et al. [28] and further modified by Takaki et al. [6] for Eqs. (4) and (5).

2.2. ⟨110⟩ tilt GB energy and mobility

Let us consider two grains shown in Fig. 3(a). We assign each grain orientation θ^α to each phase field ϕ^α as quantities independent of the evolution Eqs. (4) and (5). The GB misorientation between two grains with orientation θ^α and θ^β is determined by the relation of $\Delta\theta^{\alpha\beta} = \theta^\alpha - (\theta^\beta - 180^\circ)$ as shown in Fig. 3(b). Even if the misorientation between the neighboring grains is invariant, the microstructures within the GBs strongly depend on their inclination angle Φ as shown in Fig. 3(b) to (d). In addition, note that $\Phi = 90^\circ$ for a GB with $\Delta\theta^{\alpha\beta}$ coincides with $\Phi = 0^\circ$ for that with $180^\circ - \Delta\theta^{\alpha\beta}$ as shown in Fig. 3(d) [21]. For example, in the case of Σ3A (Σ3{111}, $\Delta\theta_{\Sigma3A} = 70.53^\circ$) system, two symmetric GBs are reduced to a coherent twin boundary for $\Phi = 0^\circ$ and to a symmetric incoherent twin boundary for $\Phi = 90^\circ$. The others except the two are asymmetric. In a polycrystalline system with arbitrary orientations, the inclination angle Φ is determined by the difference between the inclination angles $\Psi^{\alpha\beta}$ calculated from the local gradients of two phase fields of $\nabla\phi^\alpha$and $\nabla\phi^\beta$ (see Fig. 2), and the angle of a symmetrical GB plane, Φ_{sym}, as follows,

$$\Phi = \psi^{\alpha\beta} - \Phi_{sym},$$
$$\Psi^{\alpha\beta} = \tan^{-1}\left(\frac{\partial\phi^\alpha/\partial y - \partial\phi^\beta/\partial y}{\partial\phi^\alpha/\partial x - \partial\phi^\beta/\partial x}\right), \quad \Phi_{sym} = \frac{\theta^\alpha + (\theta^\beta - 180^\circ)}{2}. \tag{7}$$

The misorientation dependence of GB energy for pure Al can be provided from MD simulations, which are shown as square symbols in Fig. 4(a). You see there that the maximum value of GB energy γ_h is limited to 0.30 J/m^2. This is based on the experimental fact [17] that the boundaries with high energy definitely prefer the lower energy structure during polycrystalline grain growth. Therefore, zero-temperature symmetric GB structures of bicrystal by MD results [29,30] do not rightly correspond to the lowest energy GB structure in the real polycrystalline materials. The GB energy in the low-angle GB region ($\Delta\theta^{\alpha\beta} < 15^\circ$, $165^\circ < \Delta\theta^{\alpha\beta}$) is modeled by the normalized Read-Shockley (RS) relation [31],

$$\gamma^{\alpha\beta}(\Delta\theta^{\alpha\beta}) = \gamma_h\frac{\Delta\theta_{low}}{15}\left(1 - \ln\frac{\Delta\theta_{low}}{15}\right), \tag{8}$$

where γ_h is the GB energy at a transition point from a low-angle GB to a high-angle, i.e. the misorientation angle $\Delta\theta = 15^\circ$ and 165°, and $\Delta\theta_{low} = \Delta\theta^{\alpha\beta}$ for $\Delta\theta^{\alpha\beta} < 15^\circ$ and also $180^\circ - \Delta\theta^{\alpha\beta}$ for $\Delta\theta^{\alpha\beta} > 165^\circ$. In addition, two low energies of CSL GB of γ_Σ are referred from MD results, and the GB energy function around CSLs is approximated by the following equation,

$$\gamma^{\alpha\beta}(\Delta\theta^{\alpha\beta}) = \gamma_\Sigma + (\gamma_h - \gamma_\Sigma)\frac{\Delta\theta_\Sigma}{10}\left(1 - \ln\frac{\Delta\theta_\Sigma}{10}\right), \tag{9}$$

where $\gamma_\Sigma = \gamma\ (\Delta\theta_{\Sigma3A})$ or $\gamma\ (\Delta\theta_{\Sigma11B})$, $\Delta\theta_\Sigma = \Delta\theta_{\Sigma3A,\ \Sigma11B} - \Delta\theta^{\alpha\beta}$ for the range of $\Delta\theta_{\Sigma3A,\ \Sigma11B} - 10^\circ < \Delta\theta^{\alpha\beta} \leqslant \Delta\theta_{\Sigma3A,\ \Sigma11B}$ and $\Delta\theta^{\alpha\beta} - \Delta\theta_{\Sigma3A,\ \Sigma11B}$ for the range of $\Delta\theta_{\Sigma3A,\ \Sigma11B} < \Delta\theta^{\alpha\beta} < \Delta\theta_{\Sigma3A,\ \Sigma11B} + 10^\circ$. Note that Σ11B is Σ11{113} and $\Delta\theta_{\Sigma11B} = 129.53^\circ$. The modeled GB energy function is indicated by the solid line in Fig. 4(a). The misorientation dependence of GB mobility in the low-angle GB region is assumed by the following equation [31],

$$M^{\alpha\beta}(\Delta\theta^{\alpha\beta}) = M_h\left[1 - \exp\left\{-5\left(\frac{\Delta\theta_{low}}{15}\right)^4\right\}\right], \tag{10}$$

where $\Delta\theta_{low}$ is the same range in Eq. (8) and M_h is the high-angle GB mobility, which is 1.36×10^{-13} m^4/Js. Since a coherent twin boundary is immobile [31,32], a low mobility near Σ3A GB region is approximated using the following equation,

$$M^{\alpha\beta}(\Delta\theta^{\alpha\beta}) = M_{min} + M_{\Sigma3A}\left[1 - \exp\left\{-5\left(\frac{\Delta\theta_{\Sigma\Sigma}}{10}\right)^4\right\}\right], \tag{11}$$

where $\Delta\theta_{\Sigma\Sigma} = \Delta\theta_{\Sigma3A} - \Delta\theta^{\alpha\beta}$ for the range of $\Delta\theta_{\Sigma3A} - 10^\circ < \Delta\theta^{\alpha\beta} \leqslant \Delta\theta_{\Sigma3A}$ and $\Delta\theta^{\alpha\beta} - \Delta\theta_{\Sigma3A}$ for the range of $\Delta\theta_{\Sigma3A} < \Delta\theta^{\alpha\beta} < \Delta\theta_{\Sigma3A} + 10^\circ$, and $M_{\Sigma3A} = (M_h - M_{min})/(1 - \exp(-5))$. The mobility function obtained from Eqs. (10) and (11) is expressed by the solid line in Fig. 4(b). For computational convenience, the misorientation range is limited to $0.5^\circ \leqslant \Delta\theta \leqslant 179.5^\circ$ and we set $M_{min} = 0.05M_m$.

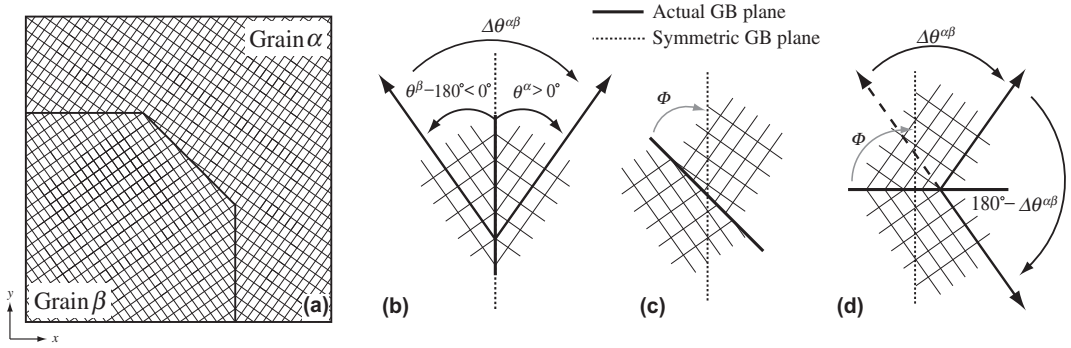

Fig. 3. (a) Schematic illustration of the orientations of two neighboring grains α and β with GB misorientation $\Delta\theta^{\alpha\beta}$ and inclination Φ, and GB structures with (b) $\Phi = 0^\circ$, (c) $\Phi = 45^\circ$, and (d) $\Phi = 90^\circ$.

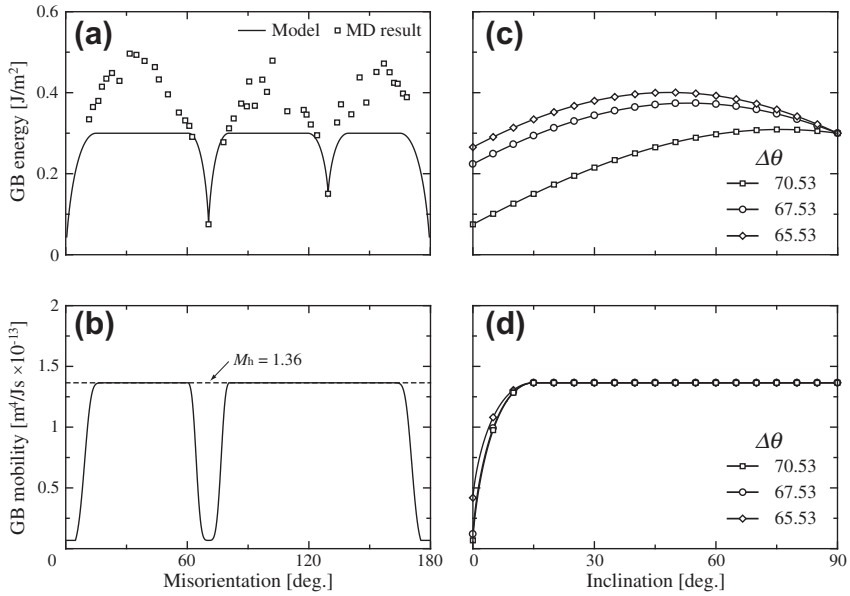

Fig. 4. Modeled functions for misorientation dependences of (a) GB energy and (b) GB mobility for pure Al, and those for inclination dependences of (c) GB energy and (d) GB mobility around Σ3A GB for pure Al as examples.

The inclination dependence of GB energy [21], which is derived from the assumption that an asymmetric GB is composed of two symmetrical GB parts of $\Phi = 0°$ and 90°, is given by

$$\gamma^{\alpha\beta}(\Phi) = \gamma_{\mathrm{I}}\cos(\Phi) + \gamma_{\mathrm{II}}\sin(\Phi). \tag{12}$$

Eq. (12) is in good agreement with energies of Σ3 and Σ11 GBs of MD simulation [21]. Two parameters in Eq. (12) of γ_{I} and γ_{II} correspond to two symmetric GB energies at $\Delta\theta = \Delta\theta^{\alpha\beta}$ and $180° - \Delta\theta^{\alpha\beta}$, respectively. For the case of Σ3 GB, $\gamma_{\mathrm{I}} = \gamma(\Delta\theta_{\Sigma 3A})$ and $\gamma_{\mathrm{II}} = \gamma(\Delta\theta_{\Sigma 3B})$, where Σ3B indicates Σ3{1 1 2} with $\Delta\theta_{\Sigma 3B} = 109.47°$. As the other examples, the inclination dependences at $\Delta\theta^{\alpha\beta} = 70.53°$, 67.53° and 65.53° are shown in Fig. 4(c), respectively. The misorientation ranges associated with the inclination dependence of GB energy are near Σ3A GB (that is, $\Delta\theta_{\Sigma 3A} - 10° < \Delta\theta^{\alpha\beta} < \Delta\theta_{\Sigma 3A} + 10°$), near Σ3B GB (that is, $\Delta\theta_{\Sigma 3B} - 10° < \Delta\theta^{\alpha\beta} < \Delta\theta_{\Sigma 3B} + 10°$), near Σ11A GB (that is, $\Delta\theta_{\Sigma 11A} - 10° < \Delta\theta^{\alpha\beta} < \Delta\theta_{\Sigma 11A} + 10°$) and near Σ11B GB (that is, $\Delta\theta_{\Sigma 11B} - 10° < \Delta\theta^{\alpha\beta} < \Delta\theta_{\Sigma 11B} + 10°$), where Σ11A indicates Σ11{3 3 2} with $\Delta\theta_{\Sigma 11A} = 50.47°$. Because the mobility of a coherent twin boundary seems to be much lower than that of other type Σ3 GBs [31,32], the inclination dependence of the GB mobility near Σ3 GB is expressed as follows:

$$M^{\alpha\beta}(\Phi) = M^{\alpha\beta}(\Delta\theta^{\alpha\beta}) + (M_{\mathrm{h}} - M^{\alpha\beta}(\Delta\theta^{\alpha\beta}))\frac{\Phi_{\mathrm{w}}}{15}\left(1 - \ln\frac{\Phi_{\mathrm{w}}}{15}\right). \tag{13}$$

where $\Phi_{\mathrm{w}} = \Phi$ around Σ3A GB, and $90° - \Phi$ around Σ3B GB region (see Fig. 4(d)).

2.3. Smoothed anisotropic function for inclination dependence of GB energy

Since the inclination angle ranges from 0° to 360° for a two-dimensional case, Eq. (12) should be applied to the MPF model as the following form:

$$\gamma^{\alpha\beta}(\Phi) = \gamma_{\mathrm{I}}|\cos(\Phi)| + \gamma_{\mathrm{II}}|\sin(\Phi)|. \tag{14}$$

This form has a cusp at $\Phi = q\pi/2$ (where q is an integer) as the solid line in Fig. 5, and thus the first derivative of Eq. (14) with respect to Φ, $(\gamma^{\alpha\beta}(\Phi))'$, never be uniquely determined. Aspiring for the continuous and differential $\gamma^{\alpha\beta}(\Phi)$ along all the range by circumventing the cusp [33], the following smoothed anisotropic function $\gamma_{\mathrm{s}}(\Phi)$ is proposed.

$$\gamma_{\mathrm{s}}(\Phi) = \begin{cases} (\gamma_{\mathrm{I}} + C_1\frac{1-\cos(\Phi)}{2})\cos(\Phi) + \frac{\gamma_{\mathrm{II}}\Phi_{\mathrm{m}}}{2} & \text{if } 0° \leqslant \Phi \leqslant \Phi_{\mathrm{m}} \\ \gamma_{\mathrm{I}}\cos(\Phi) + \gamma_{\mathrm{II}}\sin(\Phi) & \text{if } \Phi_{\mathrm{m}} < \Phi < 90° - \Phi_{\mathrm{m}} \\ (\gamma_{\mathrm{II}} + C_2\frac{1-\sin(\Phi)}{2})\sin(\Phi) + \frac{\gamma_{\mathrm{I}}\Phi_{\mathrm{m}}}{2} & \text{if } 90° - \Phi_{\mathrm{m}} \leqslant \Phi \leqslant 90° + \Phi_{\mathrm{m}} \\ -\gamma_{\mathrm{I}}\cos(\Phi) + \gamma_{\mathrm{II}}\sin(\Phi) & \text{if } 90° + \Phi_{\mathrm{m}} < \Phi < 180° - \Phi_{\mathrm{m}} \\ -(\gamma_{\mathrm{I}} + C_1\frac{1+\cos(\Phi)}{2})\cos\Phi) + \frac{\gamma_{\mathrm{II}}\Phi_{\mathrm{m}}}{2} & \text{if } 180° - \Phi_{\mathrm{m}} \leqslant \Phi \leqslant 180° \end{cases}, \tag{15}$$

and also its first derivative as,

$$\gamma_{\mathrm{s}}'(\Phi) = \begin{cases} \frac{C_1}{2}\sin(\Phi)\cos(\Phi) - (\gamma_{\mathrm{I}} + C_1\frac{1-\cos(\Phi)}{2})\sin(\Phi) & \text{if } 0° \leqslant \Phi \leqslant \Phi_{\mathrm{m}} \\ -\gamma_{\mathrm{I}}\sin(\Phi) + \gamma_{\mathrm{II}}\cos(\Phi) & \text{if } \Phi_{\mathrm{m}} < \Phi < 90° - \Phi_{\mathrm{m}} \\ -\frac{C_2}{2}\sin(\Phi)\cos(\Phi) + (\gamma_{\mathrm{II}} + C_2\frac{1-\sin(\Phi)}{2})\cos(\Phi) & \text{if } 90° - \Phi_{\mathrm{m}} \leqslant \Phi \leqslant 90° + \Phi_{\mathrm{m}} \\ \gamma_{\mathrm{I}}\sin(\Phi) + \gamma_{\mathrm{II}}\cos(\Phi) & \text{if } 90° + \Phi_{\mathrm{m}} < \Phi < 180° - \Phi_{\mathrm{m}} \\ \frac{C_1}{2}\sin(\Phi)\cos(\Phi) + (\gamma_{\mathrm{I}} + C_1\frac{1+\cos(\Phi)}{2})\sin(\Phi) & \text{if } 180° - \Phi_{\mathrm{m}} \leqslant \Phi \leqslant 180° \end{cases} \tag{16}$$

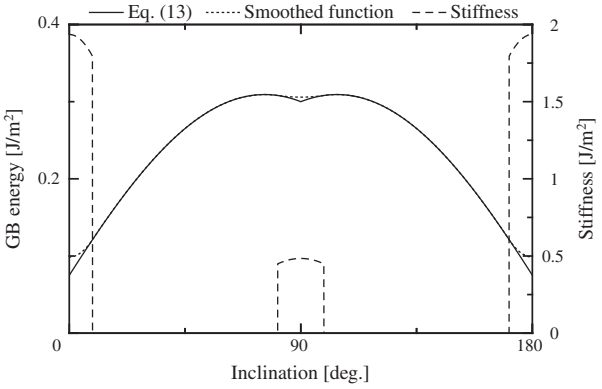

Fig. 5. Three functions of the inclination Φ in the case of Σ3A system as an example. Solid line: $\gamma(\Phi)$ of Eq. (14). Dotted line: smoothed anisotropic function $\gamma_{\mathrm{s}}(\Phi)$. Dashed line: stiffness $\gamma_{\mathrm{s}}(\Phi) + \gamma_{\mathrm{s}}''(\Phi)$. A large smoothing angle $\Phi_{\mathrm{m}} = \pi/20$ is used here to make the difference between $\gamma(\Phi)$ and $\gamma_{\mathrm{s}}(\Phi)$ visible.

where $C_1 = \gamma_{II}/\sin(\Phi_m/2)$ and $C_2 = \gamma_I/\sin(\Phi_m/2)$ express the continuity of $\gamma_s(\Phi)$ and $\gamma'_s(\Phi)$ at $\Phi = \Phi_m$, $90^\circ \pm \Phi_m$ and $180^\circ - \Phi_m$, where $\Phi_m = \pi/200$ is a parameter for smoothing within assuring stable grain growth. The applied inclination dependence of GB energy with the above anisotropic function for Σ3A is illustrated by the dotted line in Fig. 5. Remind that $\gamma''_s(\Phi)$ is not continuous at the above inclination angles, and that this function different from the conventional ones in Refs. [33,34] suggests that its stiffness $\gamma_s(\Phi) + \gamma''_s(\Phi)$ is exactly zero except near the cusps as shown by the dashed line in Fig. 5.

3. Verifications of proposed MPF model

3.1. Equilibrium shape for an isolated grain

The present MPF model is applied to a problem on an equilibrium shape of an isolated circular grain 1 surrounded by grain 2. The grain 1 is obviously disappeared as the evolution if grain growth is driven by only GB curvature. Thus, the difference in free energy density ΔE^{12} (=u) between grains 1 and 2 is employed as another driving force here. u is set up as follows: Firstly, u is equal to γ_h/R^1, where R^1 is radius of grain 1 at the initial state. As Eq. (5) is integrated in time, the GB migration rate along the x axis of V_x is computed at regular constant time increments. u is artificially decreased when $V_x > 0$ and, vice versa, u is increased when $V_x < 0$. The increment of u of Δu is divided by a constant $K > 1$ whenever V_x changes the sign. The above procedure is repeated as long as Δu is larger than the prescribed value of $(\Delta u)_{min}$. On the other hand, the analytical equilibrium shape [35] is, for comparison, given by

$$\begin{aligned} \bar{x} &= x \times u_{eq} = \gamma_s \cos(\Phi) - \gamma'_s \sin(\Phi), \\ \bar{y} &= y \times u_{eq} = \gamma_s \sin(\Phi) + \gamma'_s \cos(\Phi), \end{aligned} \tag{17}$$

where u_{eq} is the difference in free energy density between grains 1 and 2 at the equilibrium state. Also, the GB configurations obtained from numerical results of x_{num} and y_{num}, are normalized by $x_{num} \times u_{eq}$ and $y_{num} \times u_{eq}$, respectively.

To confirm the above-mentioned convergence process to the equilibrium state, the numerical simulations combing with the inclination dependences of GB energy in Eqs. (18) and (19) are performed as reference.

$$\gamma(\Phi) = \gamma_0(1 + g_{D1}\cos(4\Phi)), \tag{18}$$

$$\gamma(\Phi) = \gamma_0(1 + g_{D2}(|\cos(\Phi)| + |\sin(\Phi)|)), \tag{19}$$

where γ_0 is a constant, g_{D1} is the magnitude of which sets the degree of anisotropy [34], and g_{D2} is the cusp amplitude [33]. The following numerical conditions are used; time step $\Delta t = 0.01$ s; GB thickness $\delta_{gb} = 7\Delta x$. All simulations are carried out on the domain of $128\Delta x \times 128\Delta y$ under the grid spacing of $\Delta x = \Delta y = 0.1$ μm. The zero Neumann boundary conditions are imposed to all directions. The comparisons between the analytical equilibrium shape (solid lines) and numerical results (symbols) for the cases of $A(\gamma_0 = 0.30,\ g_{D1} = 0.050)$, $B(\gamma_0 = 0.10,\ g_{D2} = 1.00)$ and $C(\gamma_0 = 0.10,\ g_{D2} = 0.50)$ are shown in Fig. 6(a), which represent one-fourth of the numerical domain due to their symmetry. There is a smooth GB in the range of $\gamma_s(\Phi) + \gamma''_s(\Phi) > 0$ throughout the evolution and the analytical equilibrium shapes are well reproduced. For the case with Eq. (14) at $\Delta\theta = 70.53^\circ$ (Σ3A), 67.53° and 65.53° under the GB inclination dependence in Fig. 4(c) and (d), one-fourth shapes of both the numerical and the analytical results are shown in Fig. 6(b). The GB corner appears in the ranges of $\gamma_s(\Phi) + \gamma''_s(\Phi) = 0$ and as a result, the rectangular grain is formed by only flat GBs consisting of the longer low-energy and the shorter high-energy GBs. In particular, the shape of Σ3 grain reproduces the butt-type twins in grain 2, where two parallel Σ3A twins plane stopped in the middle of grain 1 at a Σ3B twin boundary, as experimentally observed [36]. Also, the Σ3A and Σ3B faces are in good agreement with the analytical equilibrium shape but the upper GBs in the other cases are not (see Fig. 6(b)). The deviation in the other cases is explained as follows; recall that $(\gamma_s + \gamma''_s)/R$ is generally defined as the driving force by only GB curvature for grain growth accompanying the inclination dependence of GB energy where R is curvature radius [35]. Thereby, u is equal to $(\gamma_s + \gamma''_s)/R$ at an equilibrium state. The preferential control of V_x does not lead the equilibrium position of the upper GB segment since $\gamma_s + \gamma''_s$ has different values at $\Phi = 0^\circ$ and 90°. Whenever $u > (\gamma_s + \gamma''_s)/R$, the upper GB form its curvature outside grain 1. The larger curvature radius occurs easily at the longer GB and lowers the driving force for shrinkage of grain 1. Crossly, the small curvature radius of Σ3B GB creates the large driving force and allows itself to stay at the equilibrium position. Consequently, it is found that the present MPF model can reproduce well the analytical shape of the isolated grain surrounded by Σ3 GB.

3.2. TJ behaviors and effect of the higher-order term

Firstly, to reveal simply an advantage of the proposed higher-order term beforehand, the free energy density distributions with respect to energy barrier of $f_b = \sum_{\alpha<\beta}^{3} W^{\alpha\beta}\phi^\alpha\phi^\beta + \sum_{\alpha<\beta<\chi}^{3} W^{\alpha\beta\chi}\phi^\alpha\phi^\beta\phi^\chi$ with $\gamma^{12} = \gamma^{13} = \gamma_A$ and $\gamma^{23} = \gamma_A/25$ is shown in Fig. 7(a) and (b), which coincide with the cases of $W^{\alpha\beta\chi} = 0$ and $W^{\alpha\beta\chi} \neq 0$, respectively. f_b is larger as its contour is darker. The vertices, edges and inside area of the equilateral triangle represent areas of each grain, GB and TJ, respectively. When $W^{\alpha\beta\chi} = 0$, f_b is almost same at the ϕ^1–ϕ^2 and ϕ^1–ϕ^3 edges and inside area of the triangle (see Fig. 7(a)), but the

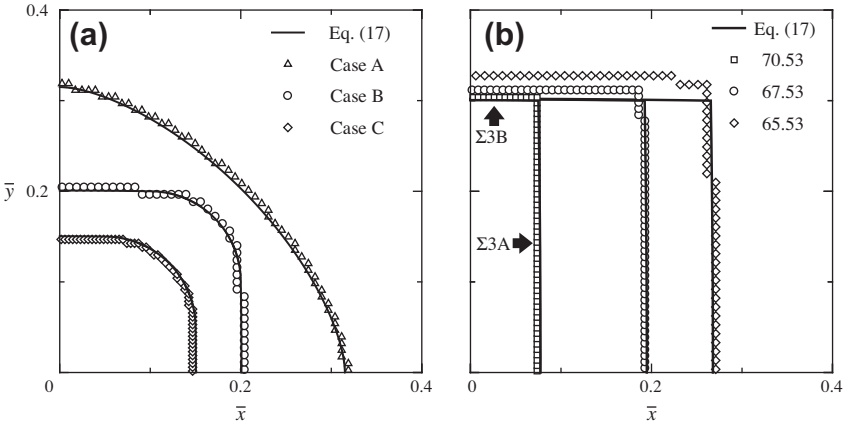

Fig. 6. The comparison with numerical results (symbols) and analytical equilibrium shape (solid lines) for (a) cases A, B and C, and (b) at $\Delta\theta = 70.53^\circ$ (Σ3A), 67.53° and 65.53°.

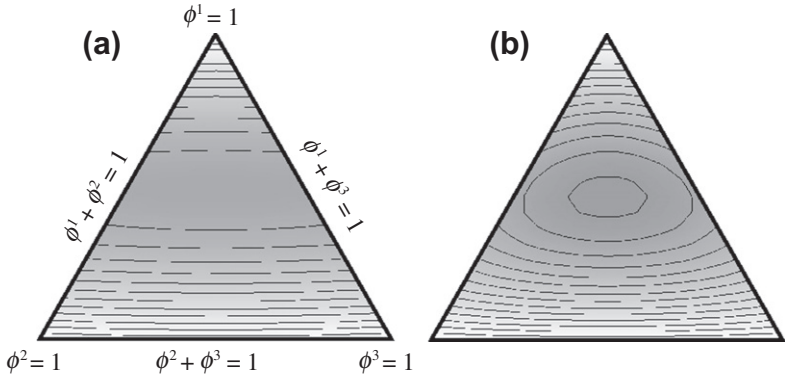

Fig. 7. Distribution of f_b at the condition with GB energy of $\gamma^{12} = \gamma^{13} = \gamma_A$ and $\gamma^{23} = \gamma_A/25$ (a) without and (b) with the higher-order term.

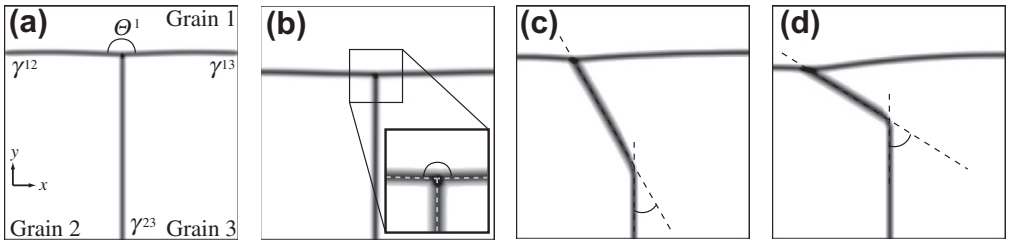

Fig. 8. (a) Initial GB configuration of isolated T-shaped TJ model with GB energies of $\gamma^{12} = \gamma^{13} = \gamma_A$ and $\gamma^{23} = \gamma_A/25$. Snapshot of TJ behavior (b) without and with the inclination dependence at Φ_{sym} = (c) 30° and (d) 60°. The angular measurement of the inset in (b) is carried out along the dashed lines via the center of the counter.

local maximum of f_b appears clearly at the inside area when $W^{\alpha\beta\chi} \neq 0$ (see Fig. 7(b)), which improves the convergence of TJ area. This fact, as a consequence, allows for more stable numerical simulation than the conventional MPF model even if the large difference between GB energies at a TJ is present.

In the second place, to investigate TJ behaviors by the present MPF model, an isolated T-shaped TJ model is prepared as shown in Fig. 8(a). Its domain size and resolution are the same as Section 3.1. As the simplest case, the following simulations are carried out with the above-mentioned GB energy condition and no difference in free energy density between grains ($\Delta E^{\alpha\beta} = 0$). To evaluate the effect of the inclination dependence on TJ behaviors, the parameters representing the inclination dependence of a 2–3 GB are set to $\Phi_{sym} = 30°$ or 60°, $\gamma_I = \gamma_A/25$, $\gamma_{II} = \gamma_A$ and the inclination-dependent mobility of Σ3A system as shown in Fig. 4(d). Other numerical conditions and boundary conditions are the same as in Section 3.1.

When the GBs are independent of their inclination, the TJ moves down due to the decrease of the curvature with γ_A (see Fig. 8(b)). Then, the TJ demonstrates the steady-state motion and the TJ angle reduces to approximately 177° from the angular measurements of the inset in Fig. 8(b). This is in almost agreement with the theoretical TJ angle of $\Theta^1 = \cos^{-1}\frac{(\gamma^{23})^2 - 2\gamma_A^2}{2\gamma_A^2} = 177.03°$ obtained from the Young's relation [18], which is valid only for the case of ignoring GB inclination. On the other hand, when one of the GBs depends on its inclination for comparison, the TJ does not hold the Young's relation evidently (see Fig. 8(c) and (d)). The effect of the inclination dependence contributes predominantly to their kinetics from the results of the preferential increase in the lower energy plane of the 2–3 GB. In addition, although the slopes of the 2–3 GB at both cases are approximately 29° and 57°, respectively, their slight deviation from Φ_{sym} results from the force balance at the TJ. Thus, it is demonstrated that the inclination dependence can be a key factor leading the characterizations of TJ behavior although its effects has frequently been ignored in experimental measurements of GB energies using tricrystals [37] and polycrystals [18,23].

4. Polycrystalline grain growth simulations

4.1. Computational model and numerical conditions

The polycrystalline grain growth simulations, combined with ⟨1 1 0⟩ tilt GB energy and mobility as shown in Fig. 4, are performed under $\Delta E^{\alpha\beta} = 0$ in order to make clear of only the effects of the inclination dependence of GB energy and mobility for single-phase pure Al. The two typical cases of A and B are compared, which correspond to those with and without the inclination dependence, respectively. The initial structure is constructed where the GB misorientations are categorized into the twin-like angle GBs (that is, $|\Delta\theta - \Delta\theta_{\Sigma 3A,\Sigma 3B}| < 3°$), GBs with low GB energy including low angles (that is, $\Delta\theta < 15°$, $165° < \Delta\theta$) and GBs with high GB energy other than the above GBs as shown in Fig. 9(a) and their orientation distributions are obtained by rotated randomly around [1 1 0] tilt axis (see Fig. 9(b)). The GBs in the above-mentioned category are called Σ3 GB, L GB and H GB below, respectively. The domain containing about 2000 grains is divided as $1024\Delta x \times 1024\Delta y$, and other computational conditions are the same as in Chapter 3. A periodic boundary condition is imposed to all directions.

4.2. Results and discussion

The obtained GB configurations are classified into three GB categories as illustrated in Fig. 9, and the configuration maps during grain growth evolutions in the cases of A and B are shown in Figs. 10 and 11, respectively. Grain coarsening rapidly proceeds at the early stages in both cases (see Figs. 10(a), (b) and 11(a), (b)), and at the later stages (Figs. 10(c), (d) and 11(c), (d)), the microstructure evolutions slow down due to the decrease in the GB regions. Throughout those evolutions, Σ3 GB (black thick lines) and L GB (light gray lines) grow noticeably at the expense of H GB (gray lines) to reduce the total system energy. However, comparison between Figs. 10(e) and 11(e) gives us a major difference on

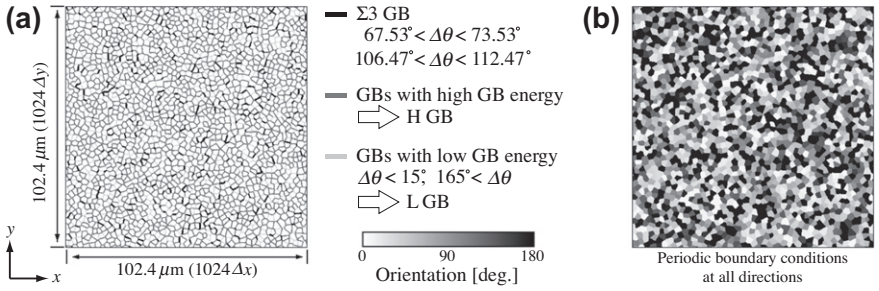

Fig. 9. (a) GB configuration and (b) grain orientation distribution rotated randomly around [1 1 0] tilt axis at an initial state in polycrystalline Al models.

Fig. 10. GB configuration maps during grain growth evolutions in the case of A after (a) 100,000, (b) 300,000, (c) 500,000 and (d) 700,000 steps and (e) orientation distribution of (d).

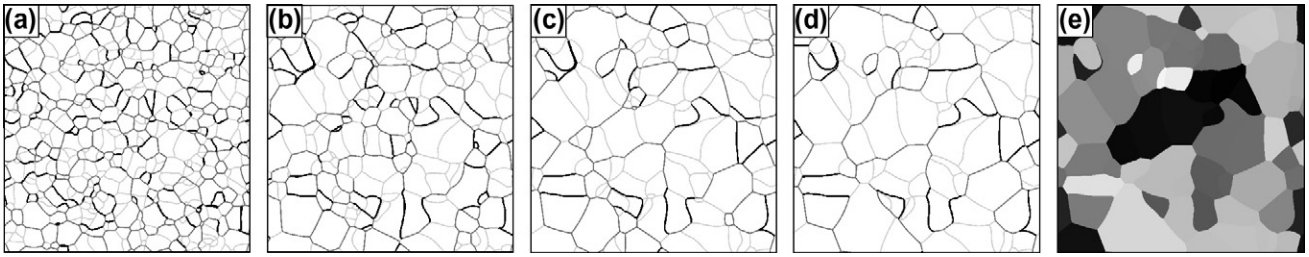

Fig. 11. GB configuration maps during grain growth evolutions in the case of B after (a) 100,000, (b) 300,000, (c) 500,000 and (d) 700,000 steps and (e) orientation distribution of (d).

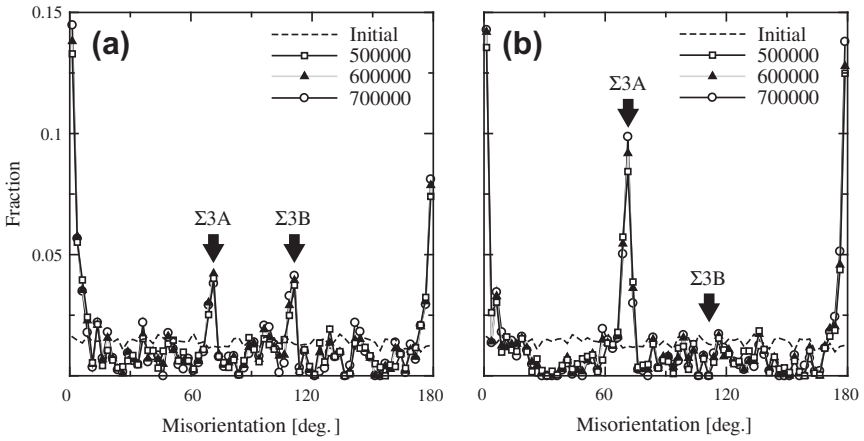

Fig. 12. Misorientation distributions at the initial state and at some later stages of (a) case A and (b) case B.

the formation of Σ3 GBs with no curvature, which causes a weak anisotropy of the microstructure in the case of A.

Misorientation distributions at the initial state and at some later stages of the two cases with the inclination dependence A and without the inclination dependence B are shown in Fig. 12(a) and (b), respectively. The fraction of the GB misorientation has three peaks at Σ3A and two L GBs in the case of B, and it inversely correlates with the ⟨1 1 0⟩ tilt GB energy valleys as shown in Fig. 4(a). In other words, the fraction of low-energy GBs increases remarkably, which is similar to the previous grain growth

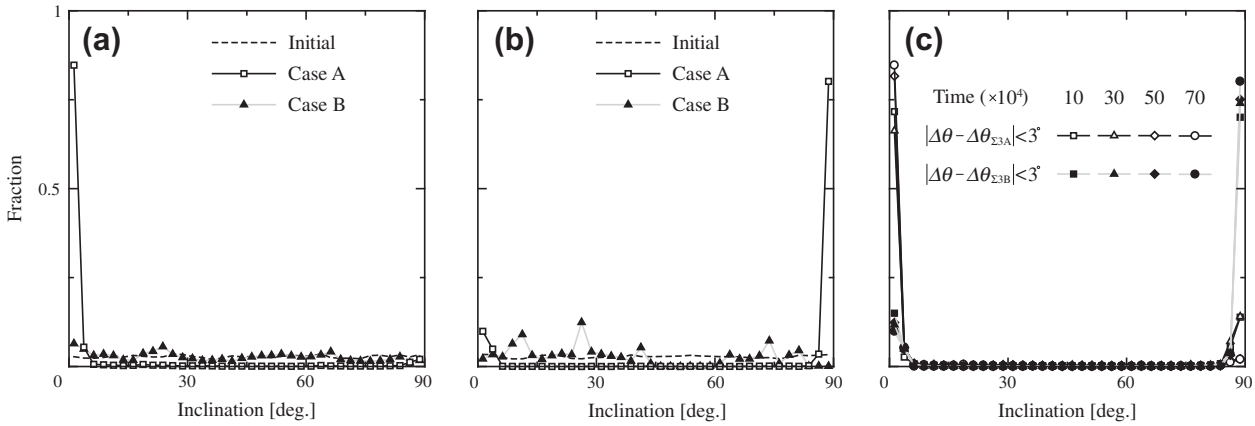

Fig. 13. Inclination distributions of GBs in the range of (a) $|\Delta\theta - \Delta\theta_{\Sigma 3A}| < 3^\circ$ and (b) $|\Delta\theta - \Delta\theta_{\Sigma 3B}| < 3^\circ$ in the cases of A and B after 700,000 steps. (c) Inclination distribution of Σ3 GB in the course of the evolution in the case of A.

simulations [8–15]. On the other hand, the appearance of the new peak of Σ3B GB is seen in the case of A (see Fig. 12(a)). This suggests that the effect of inclination dependence might allow that behavior regardless of the high-energy Σ3B observed in Fig. 4(a).

Inclination distributions of GBs in the range of $|\Delta\theta - \Delta\theta_{\Sigma 3A,\Sigma 3B}| < 3^\circ$ in the cases of A and B are shown in Fig. 13(a) and (b), respectively. You can see that almost of the inclination angle for $|\Delta\theta - \Delta\theta_{\Sigma 3B}| < 3^\circ$ is 90° in Fig. 13(b), i.e. this is crystallographically equivalent to the low-energy GB for $|\Delta\theta - \Delta\theta_{\Sigma 3A}| < 3^\circ$ at $\Phi = 0^\circ$. The low-energy GB plane of Σ3A GB is prominent in the case of A from Fig. 13(a) and it is always preferred in the course of the evolution (see Fig. 13(c)). However, the case of B with no inclination effect never produces such peaks at $\Phi = 0^\circ$ and 90° and have no outstanding characteristic. These results, in conclusion, tell us that the inclination dependence can effectively drive the GBs with low GB energy like the low-angle GB during grain growth. Since a Σ3A GB is not the lowest GB energy in Al, as shown in Fig. 4(a), the low-angle GBs prevents the growth of Σ3 GB at a TJ, regardless of the much contribution of inclination effect to TJ, as shown in Fig. 8(c) and (d). Recent experimental result [17] quantitatively supports this consideration. Further, the present grain growth model would predict the preferential grain growth driven by Σ3A GB in Cu because Σ3A (Σ3{1 1 1} twin boundary) GB energy is almost lowest in ⟨1 1 0⟩ tilt GBs.

5. Conclusions

The MPF model with a higher-order term representing energetic penalty for multiple junctions was proposed to predict the grain growth accompanying the inclination dependence of GB energy and mobility. The inclination effect was introduced on the basis of GB energy obtained from MD simulations and was successfully modified as the applicable form to the present model by replacing the discontinuity of γ' at the cusps with the smoothed anisotropic function γ_s around them. The preliminary grain growth simulation of an isolated grain surrounded by Σ3 GB certified that the analytical equilibrium shapes were well reproduced. The augmented higher-order term added to conventional MPF model could improve convergence and stability of numerical calculations around TJ region even if there exists the large GB energy gap at the TJ. Moreover, the present MPF model could realize well the Young's relation with no GB inclination effect and further extended to the case with that effect. For the polycrystalline grain growth simulations with the GB energy distribution according to the misorientation angle of Al ⟨1 1 0⟩ tilt GB, Σ3 GB inclination lead the weak anisotropy characterized by Σ3{1 1 1} twin boundary. Besides, the inclination dependence could effectively drive the GBs with low GB energy like the low-angle GB during grain growth. Since a Σ3A GB was not the lowest GB energy in pure Al, the low-angle GBs prevented the growth of Σ3 GB at a TJ, regardless of the much contribution of inclination effect to TJ, which is quantitatively supported by recent experimental result.

Acknowledgements

The author (T.H.) gratefully acknowledges the financial support by the Japan Society for the Promotion of Science for Young Scientists and the author (Y.S.) does the financial support from MEXT, Japan, Grants-in-Aid for Scientific Research (S) (20226004). Also, the authors much acknowledge the useful comments from Prof. Takaki of Kyoto Institute of Technology.

References

[1] D. Jia, Y.M. Wang, T. Ramseh, E. Ma, Y.T. Zhu, R.Z. Valiev, Appl. Phys. Lett. 79 (2001) 611–613.
[2] L. Lu, Y. Shen, X. Chen, L. Qian, K. Lu, Science 304 (2004) 422–426.
[3] Y.M. Wang, M. Chen, F. Zhou, E. Ma, Nature 419 (2002) 912–915.
[4] I. Steinbach, Modell. Simul. Mater. Sci. Eng. 17 (2009) 073001.
[5] I. Singer, H.M. Singer, Rep. Prog. Phys. 71 (2008) 106501.
[6] T. Takaki, T. Hirouchi, Y. Hisakuni, A. Yamanaka, Y. Tomita, Mater. Trans. 49 (2008) 2559–2565.
[7] T. Takaki, A. Yamanaka, Y. Higa, Y. Tomita, J. Computer-Aided Mater. Des. 14 (2007) 75–84.
[8] A. Kazaryan, Y. Wang, S.A. Dregia, B.R. Patton, Acta Mater. 50 (2002) 2491–2502.
[9] N. Moelans, B. Blanpain, P. Wollants, Phys. Rev. B 78 (2008) 024113.
[10] O.M. Ivasishin, S.V. Shevchenko, S.L. Semiatin, Acta Mater. 57 (2009) 2834–2844.
[11] N. Ma, A. Kazaryan, S.A. Dregia, Y. Wang, Acta Mater. 52 (2004) 3869–3879.
[12] A.Y. Badmos, H.J. Frost, I. Baker, Acta Mater. 51 (2003) 2755–2764.
[13] M. Upmanyu, G.N. Hassold, A. Kazaryan, E.A. Holm, Y. Wang, B. Patton, D.J. Srolovitz, Interface Sci. 10 (2002) 201–216.
[14] D.M. Kirch, E. Jannot, L.A. Barrales-Mora, D.A. Molodov, G. Gottstein, Acta Mater. 56 (2008) 4998–5011.
[15] N. Moleans, F. Spaepen, P. Wollants, Philos. Mag. 90 (2010) 501–523.
[16] L.S. Shvindlerman, V.G. Sursaeva, V.P. Yashnikov, R.G. Faulkner, Interface Sci. 2 (1994) 153–168.
[17] D.M. Saylor, B.S.E. Dasher, A.D. Rollett, G.S. Rohrer, Acta Mater. 52 (2004) 3649–3655.
[18] C.C. Yang, A.D. Rollett, W.W. Mullins, Scripta Mater. 44 (2001) 2735–2740.
[19] I. Steinbach, F. Pezzolla, B. Nestler, M. Seeßelberg, R. Prieler, G.J. Schmitz, J.L.L. Rezende, Physica D 94 (1996) 135–147.
[20] I. Steinbach, F. Pezzolla, Physica D 134 (1999) 385–393.
[21] M.A. Tschopp, D.L. Mcdowell, Philos. Mag. 87 (2007) 3871–3892.
[22] A.H. King, Scripta Mater. 62 (2010) 889–893.
[23] B. Zhao, J.Ch. Verhasselt, L.S. Shvindlerman, G. Gottstein, Acta Mater. 58 (2010) 5646–5653.
[24] K. Ko, P. Cha, D. Srolovitz, N. Hwang, Acta Mater. 57 (2009) 838–845.

[25] H. Park, D. Kim, N. Hwang, Y. Joo, C.H. Han, J. Kim, J. Appl. Phys. 95 (2004) 5515–5521.
[26] N. Ma, Q. Chen, Y. Wang, Scripta Mater. 54 (2006) 1919–1924.
[27] W. Guo, I. Steinbach, Int. J. Mater. Res. 101 (2010) 480–485.
[28] S.G. Kim, D.I. Kim, W.T. Kim, Y.B. Park, Phys. Rev. E 74 (2006) 061605.
[29] J.D. Rittner, D.N. Seidman, Phys. Rev. B 54 (1996) 6999–7015.
[30] D. Wolf, Acta Metall. Mater. 38 (1990) 781–790.
[31] F.J. Humphreys, M. Hatherly, Recrystallization and Related Annealing Phenomena, second ed., Pergamon press, Oxford, 2004.
[32] D.L. Olmsted, E.A. Holm, S.M. Foiles, Acta Mater. 57 (2009) 3704–3713.
[33] J.M. Debierre, A. Karma, F. Celestini, R. Guérin, Phys. Rev. E 68 (2003) 041604.
[34] J.J. Eggleston, G.B. McFadden, P.W. Voorhees, Physica D 150 (2001) 91–103.
[35] P.W. Voorhees, S.R. Coriell, G.B. McFadden, R.F. Sekerka, J. Crystal Growth 67 (1984) 425–440.
[36] L. Xu, D. Xu, K.N. Tu, Y. Cai, N. Wang, P. Dixit, J.H.L. Pang, J. Miao, J. Appl. Phys. 104 (2008) 113717.
[37] G. Hasson, J.Y. Boos, I. Herbeuval, M. Biscondi, C. Goux, Surf. Sci. 31 (1972) 115–137.